

# Architecture representations for quantum convolutional neural networks

Matt Lourens,<sup>1,\*</sup> Ilya Sinayskiy,<sup>1,2</sup> Daniel K. Park,<sup>3,4</sup> Carsten Blank,<sup>5</sup> and Francesco Petruccione<sup>6,1,2</sup>

<sup>1</sup>*School of Chemistry and Physics, University of KwaZulu-Natal, Durban, South Africa*

<sup>2</sup>*National Institute for Theoretical and Computational Sciences (NITheCS), South Africa*

<sup>3</sup>*Department of Applied Statistics, Yonsei University, Seoul, Korea*

<sup>4</sup>*Department of Statistics and Data Science, Yonsei University, Seoul, Korea*

<sup>5</sup>*Data Cybernetics, Landsberg, Germany*

<sup>6</sup>*School of Data Science and Computational Thinking,  
Stellenbosch University, Stellenbosch, South Africa*

The Quantum Convolutional Neural Network (QCNN) is a quantum circuit model inspired by the architecture of Convolutional Neural Networks (CNNs). The success of CNNs is largely due to its ability to learn high level features from raw data rather than requiring manual feature design. Neural Architecture Search (NAS) continues this trend by learning network architecture, alleviating the need for its manual construction and have been able to generate state of the art models automatically. Search space design is a crucial step in NAS and there is currently no formal framework through which it can be achieved for QCNNs. In this work we provide such a framework by utilizing techniques from NAS to create an architectural representation for QCNNs that facilitate search space design and automatic model generation. This is done by specifying primitive operations, such as convolutions and pooling, in such a way that they can be dynamically stacked on top of each other to form different architectures. This way, QCNN search spaces can be created by controlling the sequence and hyperparameters of stacked primitives, allowing the capture of different design motifs. We show this by generating QCNNs that belong to a popular family of parametric quantum circuits, those resembling reverse binary trees. We then benchmark this family of models on a music genre classification dataset, GTZAN. Showing that alternating architecture impact model performance more than other modelling components such as choice of unitary ansatz and data encoding, resulting in a way to improve model performance without increasing its complexity. Finally we provide an open source python package that enable dynamic QCNN creation by system or hand, based off the work presented in this paper, facilitating search space design.

## I. INTRODUCTION

Machine learning with a trainable quantum circuit provides promising applications for quantum computing [1–4]. Among various parameterized quantum circuit (PQC) models, the Quantum Convolutional Neural Network (QCNN) introduced in Ref. [5] stands out due to the shallow circuit depth, absence of barren plateaus [6], and good generalization capabilities [7]. It has been applied in the study of quantum many-body systems and combine techniques from Quantum Error Correction (QEC), Tensor Networks (TNs) and deep learning. Research at this intersection has been fruitful, yielding deep learning solutions for quantum many-body problems [8–11], quantum inspired insights for deep learning [12–14] and equivalences between them [15–17]. On its own, deep learning is ubiquitous in modern society; applications span from content filtering and product recommendations to aided medical diagnosis and scientific research. Its key characteristic is the ability to learn features from raw data rather than requiring manual design from humans [18]. The success of AlexNet [19] demonstrated the power of this which caused a shift of focus from feature design to architecture design [20] and Neural Architecture Search (NAS) aims to take the natural next step in learning

network architecture [21]. Already, state of the art deep learning models has been designed automatically [20, 22–24], surpassing previous hand crafted ones. As summarized by Elsken et al. [21], there are three main categories within NAS: search space, search strategy and performance estimation strategy. NAS methods can be computationally expensive since evaluating a single architecture requires training a full model. Focusing on the first category, search space, help increase search efficiency and reduce complexity [25] which is achieved by designing a restricted space. Typically, a set of primitive operations are used as building blocks and combined to capture some design motif which constitutes a cell. Different cells are then stacked to form a full architecture. The idea is to make use of repeated motifs which are commonly seen in successfully handcrafted architectures. Interestingly, repeated motifs are also common in quantum circuit design, for example [5, 26–30]. In particular [26] demonstrate that hierarchical architectures based on tensor networks can be used to classify classical and quantum data. Similarly Cong et al. [5] use the multiscale entanglement renormalization ansatz (MERA) as an instance of their proposed QCNN and discuss generalizations for the quantum analogues of convolution and pooling operations. In this work we take inspiration from NAS and QCNNs to formulate these analog operations as directed graphs such that they can be used as primitives for QCNN architectures. Specifically the formalism encodes the architectural and operational information of

---

\* lourensmattj@gmail.com

and between primitives in a way that they can be dynamically stacked together to form QCNNs. This facilitates search space design and enable a system to automatically generate QCNN architectures that capture multiple levels of different design motifs.

The QCNN belong to the class of hybrid quantum-classical algorithms, which are parameterized quantum circuits (PQCs) executed on a quantum computer with their parameters optimized classically. In general, there are two key factors to consider when utilizing PQCs for machine learning. That is the way data is encoded (feature map) [31, 32] and choice of quantum circuit [33–35]. The goal is to find a good quantum circuit for a given feature map of a data set, and the difficulty is finding ones that are both expressive and trainable [32]. The chosen quantum circuit is referred to as ansatz and typically circuit architecture is fixed while continuous parameters such as rotation angles are optimized [2]. However, a defining characteristic of the QCNN is its circuit architecture since one of its main operations, pooling, directly effects it. This is because pooling cause a portion of available qubits to be measured and based on the outcome, unitary operations are applied to the remaining qubits. Thus restricting future convolution and pooling operations since measured qubits aren't available for consecutive layers, resulting in favourable shallow depth circuits. Furthermore, alternating architecture has been experimentally shown to effect the expressive power and quality of initialization techniques for PQCs [27]. Therefore, circuit architecture is a key component in designing QCNNs and is typically chosen manually along with a gate set that constitute the convolution and pooling operations. The power of both choices rely heavily on the specific classification task and data that is used. With the success of NAS to classical neural networks in mind, we look to explore its possible overlap with QCNNs. There are various techniques in literature focusing on generative architectures for quantum circuits, typically referred to as variable structure ansatz [2]. Of which some explore the intersection and usage of NAS, termed quantum architecture search [36, 37]. In order to be computationally feasible, these are either oriented towards specific tasks such as the variational quantum eigensolver (VQE) [38–41] and the quantum approximate optimization algorithm (QAOA) [42, 43] or impose additional constraints such as circuit topology or allowable gates [36, 37, 44, 45]. To the best of the authors' knowledge, no framework yet encapsulates architecture generation for QCNNs.

To achieve this, we formulate the QCNN as a series of directed graphs, each functioning as a primitive operation to represent convolutions, pooling and other architectural operations. These graphs capture the architectural effect of the primitives, controlled by their respective hyperparameters, in such a way that they can be dynamically stacked on top each other. The formalism serve as a language for a system to generate circuit architectures by providing a data structure that encodes QCNNs without needing to specify convolution

or pooling unitaries (circuit ansatzes). Making it easy to have a fixed set of ansatzes and enumerating the possible ways of distributing them across a circuit in the form of a QCNN. More importantly, the formalism enables the capture of design motifs on different levels. From overall architecture such as hierarchical motifs resembling reverse binary trees to alternating the distribution of unitaries across the circuit within a single layer. We show this by generating a family of QCNN architectures based on popular motifs seen in literature and benchmark them on a music genre classification dataset, GTZAN. The benchmarks show that alternating circuit architecture impacts model performance more than other components in our experiments. For example, consider the machine learning pipeline we follow in Figure 1 to classify musical genres from audio signals. We start off with a 30-second recording of some song, FIG. 1 (a) and transform it in two ways. The first, FIG. 1 (b) represents it in tabular form, by deriving standard digital signal processing statistics from the audio signal. These are given a summary in appendix B. Second, FIG. 1 (c) represents it in image form by constructing a Mel frequency spectrogram. Both datasets are benchmarked separately, with each their own data preprocessing and encoding techniques applied. For the tabular data we test Principal Component Analysis (PCA) and tree based feature selection before encoding it in a quantum state with either qubit, IQP or amplitude encoding. Only amplitude encoding is used for the image data. Once encoded, unitary ansatzes  $U_m$  and  $V_m$  are chosen for convolution and pooling primitives  $m = 1, 2, \dots, 6$  as shown in FIG. 1 (d). These ansatzes are then tested across different instances of the architecture family. Out of all these pipeline components, alternating architecture impacted model performance the most. Based on the work presented here, we provide a python package that enable the dynamic creation of QCNNs using these primitives. It serves as a tool to design QCNN search spaces and/or enumerate closely related architectures. Enabling one to experimentally determine good architectures for a specific modelling setup. For example, this can be done to find QCNNs that perform well under a specific noise or hardware configuration, which is favourable in the Noisy Intermediate-Scale Quantum (NISQ) [46] era. Furthermore, as more qubits become available, this formalism allows for a simple and practical way to up scale the same model.

The remainder of this paper is structured as follows: we complete our introduction by summarizing the main contribution of this paper. We then give some background on the related areas of research in Section II by describing quantum machine learning and quantum convolutional neural networks on a high level. Section III is the main content of the paper, containing the architectural representation and its detail. Section IV describes the experimental procedure followed to compare different machine learning components, and section V contain

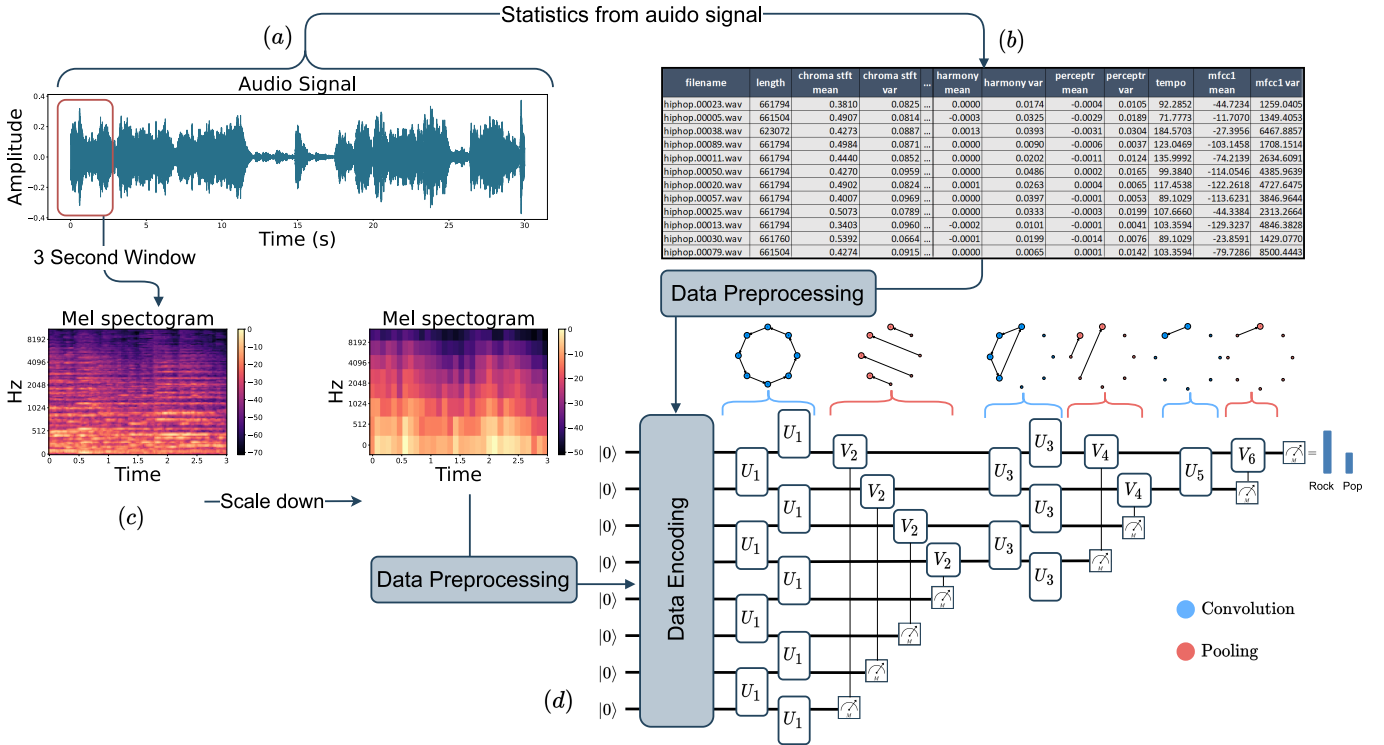


FIG. 1: High level example of the machine learning pipeline that we implemented for music genre classification. The audio signal of a song is displayed in (a). Then two forms of data are generated from the signal, namely tabular (b) and image (c) data. The QCNN circuit displayed in (d) is a specific architecture that was generated using the framework discussed in Section III (Architecture representations). It is also an example of a QCNN architecture that favours PCA, since qubits are pooled from bottom to top and principal components encoded top to bottom.

the result of those comparisons. Finally, we end with a discussion about applications and future steps in section VI.

### Overview of main results

Figure 2 shows how our work facilitate the architectural design process for QCNNs. We provide a framework, inspired by NAS, that enable automatic QCNN generation and search space design. This is seen in the code block of Figure 2 (e) and (f). These two lines of code is all that is required to generate the circuit in Figure 1 (d), explicitly capturing its motifs. This extends naturally to generating a whole family of related circuits which can be seen in Algorithm 1. The framework enables the creation of intricate and novel architectures which we show to impact model performance more than other modelling components such as circuit ansatz, data encoding, data preprocessing, data format and so on in Section V. This is achieved through providing an architectural representation for QCNNs and it's primitive operations. Consider Figure 2, the primitives such as a convolution or pooling act as level  $l = 1$  motifs encoded as directed graphs. They function as building blocks for higher level motifs similar to the hierarchical representa-

tion for DNNs by [25]. This allow the capture of modularized design patterns and repeated motifs, often seen in successfully handcrafted PQC and DNNs. The full QCNN is the highest level motif  $l = L$  which when assembled is a sequence of directed graphs. For example, a convolution followed by pooling is a level  $l = 2$  motif (a convolution-pooling unit) and repeating that three times a level  $l = 3$  motif. Encoding the architectural effect of convolutions, pooling and other primitives allow them to be dynamically stacked together by system or hand to build QCNNs and QCNN search spaces. We further provide a python package that achieves exactly this, compatible with any quantum computing framework. In summary, the contributions are: an architectural representation for QCNNs, a python package facilitating dynamic QCNN creation and experimental results illustrating the impact of alternating circuit architecture on a music genre classification dataset, GTZAN.

## II. BACKGROUND

### Quantum Machine Learning

The goal of classification is to utilize some data  $X$  alongside a function  $f_m$  (model) to accurately represent

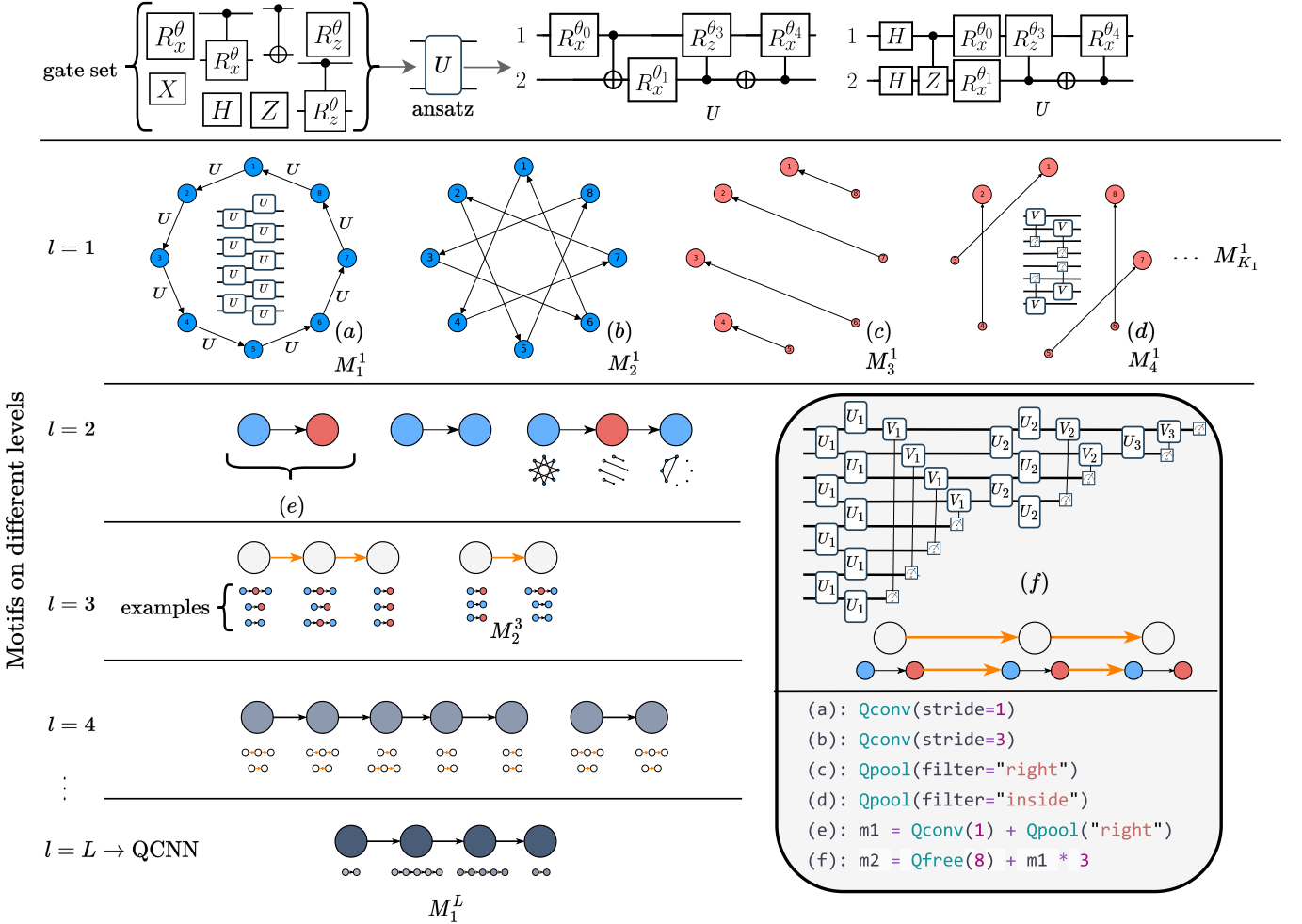


FIG. 2: Example motifs on different levels  $l$ . From a given gate set, two qubit unitaries are constructed as ansatz. Then deciding how to spread these unitaries across the circuit in the form of a QCNN is achieved with the architectural representation of motifs on different levels. On the lowest level  $l = 1$  we define primitives which act as building blocks for the architecture. For example:  $M_1^1$  is a convolution operation with stride 1,  $M_3^1$  a pooling operation with filter  $F^{right}$ , combined they form the level two motif (e): a convolution-pooling unit  $M_2^2$ . Motifs are dynamically stacked to form larger motifs until the final level  $l = L$  containing only one motif  $M_1^L$ , the full QCNN architecture. The code block showcase example usage of the python package, only lines (e) and (f) are required to generate the circuit in Figure 1 (d). The package allow for the dynamic creation of QCNN architectures by system or hand, using the architectural representation provided in this paper.

a discrete categorization  $y$ , i.e.  $f_m(X, \theta) = \hat{y} \approx y$ . The data is utilized by iteratively changing the model  $f_m$  parameters  $\theta$  based on the disparity between the current representation  $\hat{y}$  and the actual categorization  $y$ , measured with a cost function  $C(y, \hat{y})$ . Minimizing this function or learning is done until some specified critical point is reached, resulting in a set of parameters  $\theta^*$  that can be used alongside the model  $f_m$  and some new data  $X^*$  to estimate their categories. This describes a supervised type of learning, since some actual categorizations  $y$  are known beforehand. It is achieved with the aid of computers and forms part of the broader field of machine learning, whose technology is ubiquitous in modern society. One interesting realization of this

procedure is with the use of quantum computers, where the function  $f_m$  is constructed as a variational quantum circuit that acts on a quantum state  $|\psi\rangle$ . Learning  $\theta$  still makes use of classical (i.e., non-quantum) computation, resulting in a hybrid quantum-classical algorithm [47]. The hope is that the exploration of quantum circuits  $f_m$  may lead to new approaches in machine learning that would be difficult to achieve classically [48]. Variational quantum algorithms are also applicable in the NISQ era, making the exploration thereof a step forward in the development of future quantum technologies [46].

The goal is then to find a quantum circuit (often called circuit ansatz)  $f_m(X, \theta)$  that estimates  $y$  accurately while

keeping the number of required parameters  $|\theta|$  as small as possible. A popular candidate for the exploration and construction of different quantum circuits are tensor networks (TNs). This is because they may be used to represent quantum states and have had great theoretical and numerical success in the field of quantum many-body systems [49]. Within this context, tensors can be thought of as multidimensional arrays, where the rank of a tensor indicates the array's dimension. For example, scalars, vectors and matrices correspond to rank-0, rank-1 and rank-2 tensors respectively. A tensor network is also a tensor but decomposed of other, typically lower rank, tensors through contraction operations. Being able to describe high-rank tensors through low-rank tensors in a network is, in part, what makes TNs powerful (see [49] for a more rigorous explanation). Experiments applying the structure of successful TNs from quantum many-body systems to quantum circuit design for machine learning show promising results. These include structures such as matrix product states (MPS) [50], tensor tree networks (TTN) [26, 50] and the multiscale entanglement renormalization ansatz (MERA) [5, 26]. Specifically, the MERA tensor network overlaps with CNNs in terms of architecture [5, 26] and with the combination of QEC give rise to the QCNN presented in [5].

### Quantum Convolutional Neural Networks

In the classical CNN setting, a convolution refers to an operation that produces some feature map by cross correlating a kernel with a given input. The input is the previous layer, and by having the same kernel applied to all of its values result in weights being shared to the following layer. Sharing of weights is an important characteristic of a CNN, since it shapes feature maps to be translational equivariant representations of the previous layer [51]. After the convolution operation, non-linearity is introduced through an activation function. This is typically followed by a pooling operation, which down-samples the feature map to introduce local translational invariance and to reduce model complexity.

While there have been various proposals for the quantum analogue of convolutional neural networks [5, 28, 30, 52–55], our work focuses on the framework proposed by Cong et al. [5] and the findings of Grant et al. [26]. As with many of these proposals, the key components are weight sharing, sequential reduction of system size via pooling and translational invariance of convolutions. This way the QCNN (Figure 1d) implements analogous convolution and pooling operations in a quantum circuit setting. These operations are applied on a circuit architectural level, where a convolution consist of unitary operations  $U_i$  being applied to all available qubits in a given layer. It's applied to all available qubits in order to achieve a type of translational invariance and being identical unitaries allows the sharing of their weights. This

relates to a CNN applying a single kernel to all input neurons in a given layer. Weight sharing is an important characteristic of the QCNN, as it causes the magnitude of its cost function gradients to increase, which is desirable in the face of barren plateau's since it counteracts vanishing gradients [6]. Pooling consist of measuring a portion of the available qubits within a layer and then applying unitary rotations  $V_i$  to the remaining ones based on the measurement outcomes. This leads to a reduction in parameters to optimize, which introduces nonlinearity to the model while also reducing its computational overhead [5]. Convolution and pooling operations are repeated until the system size is sufficiently small. For binary classification, one of the qubits are measured, and the expectation value defined as the probability for binary class membership.

Considering the MERA structure in reverse satisfies the above description, giving rise to a valid QCNN architecture. The QCNN circuit architecture has been successfully applied to problems surrounding quantum phase recognition (QPR) and quantum error correction (QEC). The partial measurement performed during pooling relates to syndrome measurements in QEC, giving the intuition that a QCNN is viewed as some combination of MERA and QEC [5].

### III. ARCHITECTURE REPRESENTATIONS

The chosen architecture of quantum circuits [26, 27, 43] and deep neural networks [21] is an important component for their success. This is emphasized for DNNs by NAS which seek to automate that choice. To this end, a search space is required that determine which architectures are reachable by an algorithm. Effective search spaces will greatly reduce the computational complexity of the algorithm, making NAS methods feasible. Creating them requires a method of architectural representation that is able to capture design motifs on multiple levels of abstraction. DNNs have well defined primitive operations, for instance  $n \times n$  depthwise convolutions,  $n \times n$  max-pooling and many more, that can be combined dynamically to form a full model. Repeated motifs are often seen in handcrafted designs where a specific combination of primitive operations is reused throughout the model. Recent proposals in NAS [21] attempt to learn such motifs by combining primitive operations to form cells and then stack the cells in some predefined manner resulting in a full architecture. Liu et al. [25] presented a hierarchical representation where the macro architecture is also learnt by using lower level motifs as building blocks for higher level ones. Directed graphs are used to capture motifs, where edges correspond to operations and nodes to feature maps. On the lowest level primitive operations are used as edges and going up the hierarchy use previous graphs (motifs) as edges for the new graph. The highest level consists of one motif which constitutes a full architecture. This is a powerful technique that capture

modularized design patterns often seen in handcrafted architectures. Similar design patterns occur in quantum circuits and is emphasized by QCNNs. Consider Figure 2, from a gate set, unitaries are built according to some ansatz. They are then placed on the circuit according to design motifs on different levels. Lower level motifs, Figure 2 (a)-(d), such as convolutions (identical unitaries, translational invariance) and pooling (system reduction) to higher level ones such as overall architecture being hierarchical or based on tensor network structures [5, 26]. These motifs are implemented implicitly in QCNN designs and we aim to capture them explicitly so that a system can learn them. Therefore a method of architectural representation is required that can capture design motifs for QCNNs. To this end, we also use directed graphs and define primitives for QCNNs to be used as building blocks for their architecture.

### Digraph Formalism

Consider the motif levels  $l$  in Figure 2, we encode the QCNN as a sequence of directed graphs, each acting as a primitive operation that capture level  $l = 1$  motifs such as a convolution (Qconv) or pooling (Qpool). The effect of a primitive is based of its hyperparamaters and the effect of its predecessor. This way their individual and combined architectural effect is captured, enabling them to be dynamically stacked one after another to form second level  $l = 2$  motifs. Stacking these stacks in different ways constitute higher level motifs until a final level  $l = L$  where there is only one motif constituting the full QCNN architecture. We also define a special primitive Qfree that free up pooled qubits to be used again for future operations. For a primitive  $G = (Q, E)$ , its nodes  $Q$  represent available qubits, and oriented edges  $E$  the corresponding unitary applied between a pair of them. The direction of an edge indicates the order of interaction for the unitary. For example a CNOT gate with qubit  $i$  as control and  $j$  as target is represented by the edge from qubit  $i$  to qubit  $j$ . In the case of pooling, controlled unitaries are used in place of measurement due to the deferred measurement principle [56]. We define the full QCNN architecture as follow:

**Definition 1.** The  $k^{th} = 1, 2, \dots, K_l$  motif on level  $l = 1, 2, \dots, L$  is the tuple  $M_k^l = (M_j^{l-1} | j \in \{1, 2, \dots, K_{l-1}\})$ . At the lowest level  $M_k^1$  corresponds to a primitive operation which is part of the set  $M^{(1)} = \{M_1^1, M_2^1, \dots, M_{K_1}^1\}$ , for instance  $M_1^1 = Qconv(2)$ ,  $M_2^1 = Qpool(\text{right})$ , ... At the highest level  $l = L$  there is only one motif  $M_1^L$  which is a hierarchy of tuples.  $M_1^L$  is flattened through an assemble operation:  $M = \text{assemble}(M_1^L)$  which encodes each primitive into a directed graph  $G_m = (Q_m, E_m)$  where  $m$  is the index such that the full QCNN architecture is represented by  $M = (G_1, G_2, \dots, G_{|M|})$ .

Figure 2 contain examples of motifs on different levels for a QCNN. Higher level motifs are tuples and the lowest level ones directed graphs. The dependence between successive motifs is specified in the following definition:

**Definition 2.** Let  $x \in \{c, p, f\}$  indicate the primitive type for  $\{Qconv, Qpool, Qfree\}$  and  $M_1^L$  be the highest level motif for a QCNN. Then  $\text{assemble}(M_1^L)$  flattens depth-wise into  $M = (G_1, G_2, \dots, G_{|M|})$  where  $G_m = (Q_m^x, E_m^x)$ .  $G_1$  is always a  $Qfree(N_q)$  primitive specifying the number of available qubits with  $N_q$ . For  $m > 1$ ,  $G_m$  is defined as:

If  $G_m$  is a  $Qfree(N_f)$  primitive then:

$$Q_m^f = \{1, 2, \dots, N_f\}$$

$$E_m^f = \{\}$$

If  $G_m$  is a convolution primitive:

$$Q_m^c = \begin{cases} Q_{m-1}^x & \text{if } x \in \{c, f\} \\ Q_{m-1}^x \setminus \{i \in (i, j) \in E_{m-1}^x\} & \text{if } x = p \end{cases}$$

$$E_m^c = \{(i, j) | (i, j) \in Q_m^c \times Q_m^c\}$$

If  $G_m$  is a pooling primitive:

$$Q_m^p = \begin{cases} Q_{m-1}^x & \text{if } x \in \{c, f\} \\ Q_{m-1}^x \setminus \{i \in (i, j) \in E_{m-1}^x\} & \text{if } x = p \end{cases}$$

$$E_m^p = \{(i, j) | (i, j) \in Q_m^p \times Q_m^p, i \neq j,$$

$$d^-(i) = 0, d^+(i) = 1, d^-(j) \geq 1, d^+(j) = 0\}$$

with  $d^-(i)$  and  $d^+(i)$  referring to the indegree and outdegree of node  $i$ , respectively and  $\setminus$  to set difference.

Figure 3 show a three level motif implementation using both definitions. It's the same circuit from Figure 1 (d) represented through the digraph perspective. If the  $m^{th}$  graph in  $M$  is a convolution, we denote its two qubit unitary acting on qubit  $i$  and  $j$  as  $U_m^{ij}(\theta)$ . Similarly, for pooling, we notate the unitary as  $V_m^{ij}(\theta)$ . The action of  $V_m^{ij}(\theta)$  is measuring qubit  $i$  (the control) which causes a unitary rotation  $V$  on qubit  $j$  (the target). With this figure and notational scheme in mind, definition 2 read as follows:

$Q_m^x$  is the set of available qubits for the  $m^{th}$  primitive in  $M$ , where  $x \in \{c, p, f\}$  for convolution, pooling or Qfree respectively. The first primitive  $G_1$  is  $Qfree(N_q)$  which specifies the number of available qubits  $N_q$  for future operations. Any proceeding  $m > 1$  primitive  $G_m$  only has access to qubits not measured up to that point. This is the previous primitive's available qubits  $Q_{m-1}^x$  if its type  $x \in \{c, f\}$  is a convolution or Qfree. Otherwise, for pooling, it's the set difference:  $Q_{m-1}^x \setminus \{i \in (i, j) \in E_{m-1}^x\}$  when  $x = p$  since the  $i$  indices during pooling  $(i, j) \in E_m^p$  indicates measured qubits. This is visualized as small red circles in Figure 3. The only way to make those qubits available again is through  $Qfree(N_f)$ , which can be used to free up  $N_f$

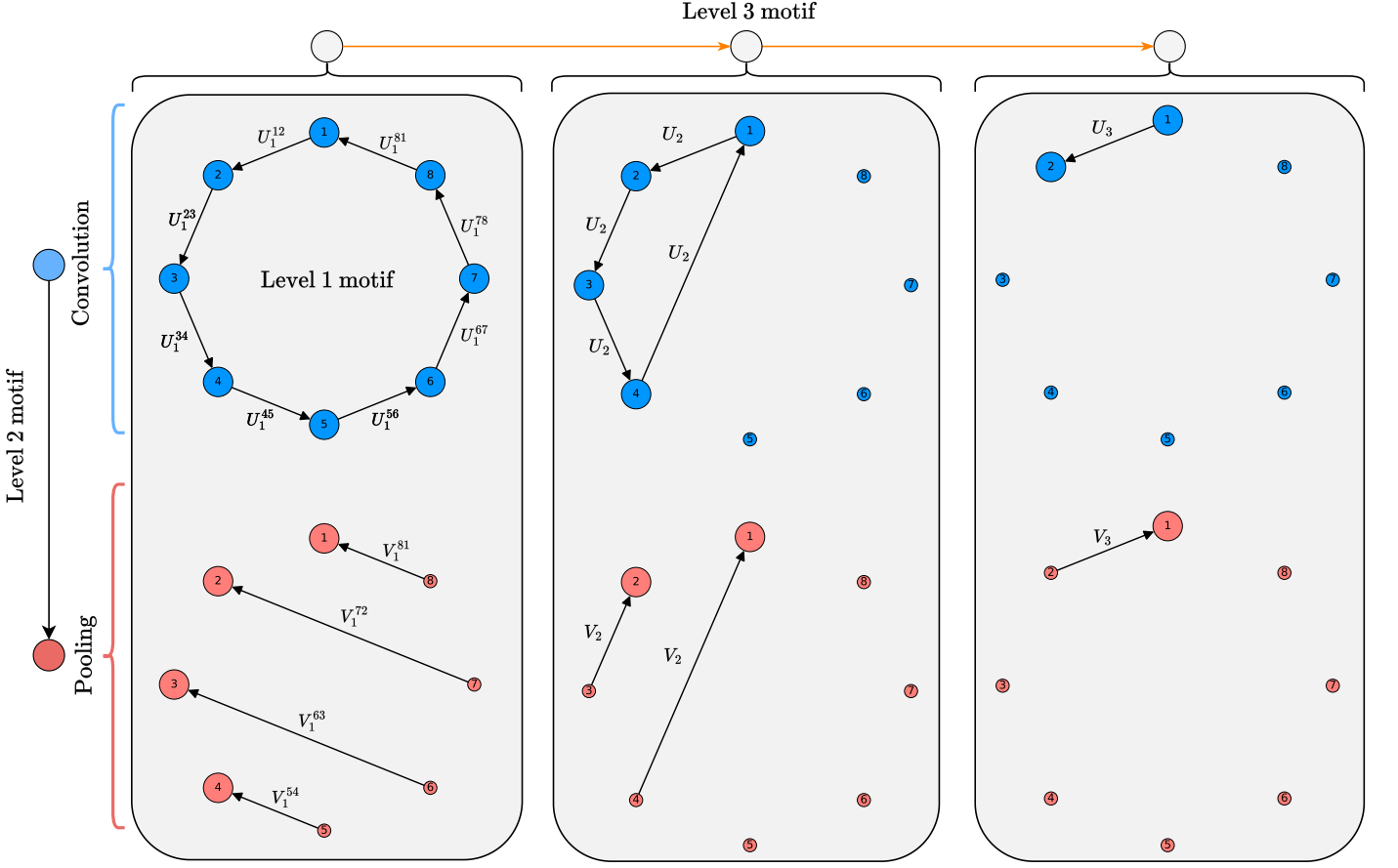


FIG. 3: Graph view for the circuit architecture in Figure 1 (d). The same two qubit unitary is used in all layers for the convolution operation, i.e.  $U_m^{ij} = U_m$ . Similarly in this example we use the same two qubit pooling unitaries  $V_m^{ij} = V_m$ . Consider layer  $l = 1$ , the top left graph is  $C_1$  with all eight qubits  $Q_1^c$  available for the convolution operations  $U_1^{ij}, (i, j) \in E_1^c$ . Below  $C_1$  is  $P_1$  with half the qubits of  $Q_1^p$  measured, indicated by the  $i^{th}$  indices of  $V_1^{ij}, (i, j) \in E_1^p$ . For example, qubit 8  $\in Q_1^p$  is measured and  $V_1$  applied to qubit 1  $\in Q_1^p$  as indicated by  $V_1^{81}, (8, 1) \in E_1^p$ . This pattern repeats until one qubit remain in  $P_3$ , which is measured and used to classify the music genre.

qubits. For the convolution primitive,  $E_m^c$  is the set of all pairs of qubits that have  $U_m^{ij}(\theta)$  applied to them. Finally for the pooling primitive,  $E_m^p$  is the set of pairs of qubits that have pooling unitaries  $V_m^{ij}(\theta)$  applied to them. The restriction being that if qubit  $i$  is measured, it cannot have any other rotational unitary  $V$  applied to it within the same primitive  $G_m$ . This means the indegree  $d^-$  of node  $i$  is zero. Similarly, if qubit  $i$  is measured it may only have one corresponding target, meaning that the outdegree  $d^+$  of node  $i$  is one. In the same vein, no target qubit  $j$  can be the control for another,  $d^+(j) = 0$ . Every target qubit  $j$  have at least one corresponding control qubit  $i$ ,  $d^-(j) \geq 1$ . It is possible for multiple measured qubits to have the same target qubit, giving  $E_m^p$  a surjective property.

Following this definition, we can express a convolution or

pooling operation for the  $m^{th}$  graph in  $M$  as:

$$\widetilde{U}_m = \prod_{(i,j) \in E_m^c} U_m^{ij}(\theta) \quad (1)$$

$$\widetilde{V}_m = \prod_{(i,j) \in E_m^p} V_m^{ij}(\theta) \quad (2)$$

Let  $\widetilde{W}_m = \widetilde{U}_m$  or  $\widetilde{V}_m$  be the  $m^{th}$  primitive in  $M$  based on whether it's a convolution or pooling and the identity  $I$  if it's a Qfree primitive. Then the state of the QCNN after one training run is:

$$|\psi\rangle = \widetilde{W}_{|M|} \cdots \widetilde{W}_4 \widetilde{W}_3 \widetilde{W}_2 \widetilde{W}_1 U_{\text{encoding}} |0\rangle \quad (3)$$

We note that the choice of  $V$  is unrestricted, which means that within one layer each  $V$  can be a different rotation. Figure 1d shows a special case where the same  $V$  is used per layer, which is computationally favourable compared to using different ones. To enable weight sharing, the QCNN require convolution unitaries to be the

same i.e.  $U_m^{ij} = U_m^{kh}$  where  $(i, j) \in (k, h) \in E_m^c$ . This formulation only regards one and two qubit unitaries for convolutions, one qubit unitaries being described with  $E_m^c = (i, i), i \in Q_m^c$ . It is possible to use  $n$ -qubit unitaries where  $n > 2$  since multiple two qubit unitaries may be used to construct any arbitrary  $n$ -qubit unitary. Although in practice mostly two qubit unitaries are used, and the focus of this paper.

After training,  $|\psi\rangle$  in eq. 3 is measured based on the type of classification task, in this work we focus on binary classification allowing us estimate  $\hat{y}$  by measuring the remaining or specified qubit in the computational basis:

$$\hat{y} = P(y = 1) = |\langle 1|\psi\rangle|^2 \quad (4)$$

We note that multi-class classification is also possible by measuring the other qubits and associating each with a different class outcome. Following this, we calculate the cost of a training run with  $C(y, \hat{y})$ , then using numerical optimization the cost is reduced by updating the parameters from Equations 1 - 2 and repeating the whole process until some local minimum is reached. Resulting in a model alongside a set of parameters to be used for classifying unseen data.

### Controlling the primitives

We define basic hyperparameters that control the individual architectural effect of a primitive. There are two broad classes of primitives, special and operational. A special primitive has no operational effect on the circuit, such as Qfree. Its purpose is to make qubits available for future operational primitives and therefore has one hyperparameter  $N_f$  for this specification.  $N_f$  is typically an integer or set of integers corresponding to qubit numberings:

$$Q_m^f = \{1, 2, \dots, N_f\} \quad \text{if } N_f \text{ is an integer} \quad (5)$$

$$Q_m^f = N_f \quad \text{if } N_f \text{ is a set of integers} \quad (6)$$

Each operational primitive has its own stride parameter analogous to classical CNNs. For a given stride  $s$ , each qubit gets paired with the one  $s$  qubits away modulo the number of available qubits. For example a stride of 1 pairs each qubit with its neighbour. This depends on the qubit numbering used which is based on the circuit topology. For illustration purposes, we use a circular topological ordering, but any layout is possible as long as some ordering is provided for  $Q_1^f$ . For the convolution primitive we define its stride  $s_c \in \{1, 2, 3, \dots\}$  as:

$$E_m^c = \{(i, (i + s_c) \bmod |Q_m^c|) | i \in Q_m^c\} \quad \text{if } |Q_m^c| > 2 \quad (7)$$

$$E_m^c = \{(i, j) | i, j \in Q_m^c, i \neq j\} \quad \text{if } |Q_m^c| = 2 \quad (8)$$

$$E_m^c = \{(i, i) | i \in Q_m^c\} \quad \text{if } |Q_m^c| = 1 \quad (9)$$

Equation (8) captures the case where there are only two qubits available for a convolution and equation (9) when there is only one which implies the convolution unitaries only consist of single qubit gates. A stride of  $s_c = 1$  is a typical design motif for PQCs and the graph formalism allow for a simple way to capture and generalize it. To achieve translational invariance for all strides the two constraints:  $|E_m^c| = |Q_m^c|$  and  $(i, j) \neq (k, h)$  where  $(i, j) \in (k, h) \in E_m^c$  are added. Another option for translational invariance is a Qdense primitive, which only differs from Qconv in that  $E_m^c$  generates all possible pairwise combinations of  $Q_m^c$ . This primitive is available in the python package but left out from the definition (because of its similarity). Figure 4 show different ways in which  $s_c$  generate  $E_m^c$  for  $|Q_m^c| = 8$ .

The pooling primitive has two hyperparameters, a stride  $s_p$  and filter  $F_m^*$ . The filter indicates which qubits to measure and the stride how to pair them with the qubits remaining. We define the filter as a binary string:

$$F_m^* = w_1 w_2 \cdots w_{|Q_m^p|} \quad \begin{cases} w_i = 1 & \text{if qubit } i \text{ is measured} \\ w_i = 0 & \text{otherwise} \end{cases} \quad (10)$$

For  $N = 8$  qubits, the binary string  $F_m^* = 00001111$  translates to measuring the rightmost qubits, i.e.  $\{i | i \in Q_m^p, i \geq 5\}$ . Figure 3 is an example where the pattern  $F_2^* = 00001111 \rightarrow F_4^* = 0011 \rightarrow F_6^* = 01$  is used, visually the qubits are removed from bottom to top. Encoding filters as binary strings is useful since generating them becomes generating languages, enabling the use of computer scientific tools such as context free grammars and regular expressions to describe families of filters. Pooling primitives enable hierarchical architectures for QCNNs and in section III (search space design) we illustrate how they can be implemented to create a family resembling reverse binary trees. The action of the filter is expressed as:  $F_m^* \star Q_m^p = Q_{m+1}^x$  where  $\star$  slices  $Q_m^p$  corresponding to the 0 indices of  $F_m^*$ , i.e.  $w_i = 0$  (not measured). For example  $010 \star \{4, 7, 2\} = \{4, 2\}$ . This example illustrates the case where an ordering was given to the set of available qubits to represent some specific topology of the circuit. Let  $Q_{m+1}^x = F_m^* \star Q_m^p$  then the pooling primitive stride  $s_p = \{1, 2, \dots\}$  is defined as:

$$E_m^p = \{(i, (j + s_p) \bmod |Q_{m+1}^x|) | i \in Q_m^p \setminus Q_{m+1}^x, j \in Q_{m+1}^x\} \quad (11)$$

### Search Space Design

We show how the digraph formalism facilitates QCNN generation and search space design. Grant et al. [26] exhibit the success of hierarchical designs that resemble reverse binary trees. To create a space of these architectures we only need three levels of motifs. The idea is to

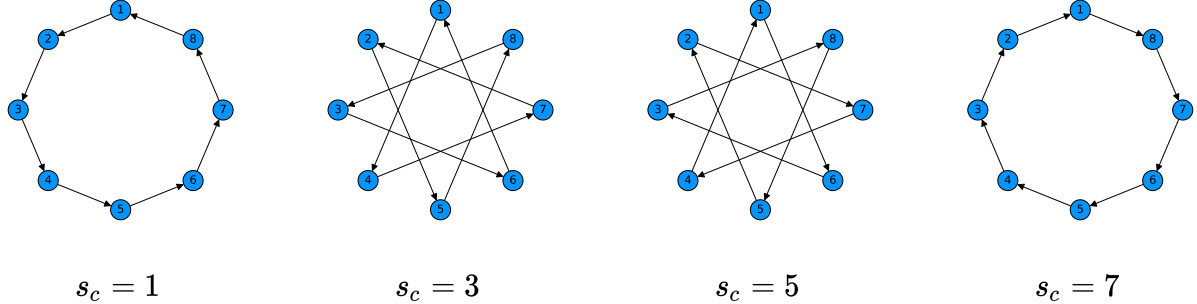


FIG. 4: Diagram showing how changing the convolution stride  $s_c$  generates different configurations for  $E_m^c$ .

reduce the system size in half until one qubit remain while alternating between convolution and pooling operations. Given  $N$  qubits, a convolution stride  $s_c$ , pooling stride  $s_p$  and a pooling filter  $F^*$  that reduce system size in half, a reverse binary tree QCNN is generated in algorithm 1.

---

**Algorithm 1** QCNN, reverse binary tree architecture

---

**Input:**  $N, s_c, s_p, F^*$

**Output:** QCNN  $\rightarrow M = (G_1, G_2, \dots, G_{|M|})$

▷ Primitives:

$$M_1^1 \leftarrow \text{Qconv}(\text{stride} = s_c)$$

$$M_2^1 \leftarrow \text{Qpool}(\text{stride} = s_p, \text{filter} = F^*)$$

▷ Motif: alternate convolution and pooling

$$M_1^2 \leftarrow M_1^1 + M_2^1$$

▷ Motif: repeat until one qubit remain

$$M_1^3 \leftarrow \text{Qfree}(N) + M_1^2 \times \log_2 N$$

$$M \leftarrow \text{assemble}(M_1^3)$$


---

It shows how instances of this architecture family can be created. Two primitives are defined on level one, convolution and pooling, which are sequentially combined on level two as  $M_1^2$  to form a convolution-pooling unit. This second level motif is repeated until the system size is one which is  $\log_2(N)$  times for  $N$  qubits, since  $F^*$  is chosen to reduce system size in half. The addition and multiplication operations act as append and extend for tuples. For example  $M_1^l + M_2^l = (M_1^l, M_2^l)$  and  $M_k^l \times 3 = (M_k^l, M_k^l, M_k^l)$  which allow for an intuitive way to build motifs. It's easy to expand the algorithm for more intricate architectures, for instance increasing the number of motifs per level and the number of levels. A valid level four motif for algorithm 1 would be  $M_1^4 = (M_1^3 + M_2^3) \times 3$ , where  $M_2^3 = \text{Qfree}(4) + M_2^2 + M_2^1$  and  $M_2^2 = M_1^1 \times 2$  which is the reverse binary tree architecture  $M_1^3$  then two convolutions and one convolution-pooling unit on four qubits, all repeated three times. Motifs can also be randomly selected on each level to generate novel architectures. The python package we provide act as a tool to facilitate architecture generation exactly this way.

We now analyze the family of architectures generated by

algorithm 1 in more detail. First we consider the possible pooling filters  $F^*$  that reduce system size in half. It's equivalent to generating strings for the language  $A = \{w | w \text{ has an equal number of 0s and 1s}, |w| = |Q_m^p|\}$ . Let  $N_{m-1} = |Q_{m-1}^x|$  indicate the number of available qubits for the filter  $F_m^*$ . Then based on the  $\binom{4}{2} = 6$  possible equal binary strings [57] of length 4 we construct the following *pooling filters*:

$$F_m^{\text{right}} = \{0^{\frac{n}{2}} 1^{\frac{n}{2}} | n = N_{m-1}\} \quad (12)$$

$$F_m^{\text{left}} = \{1^{\frac{n}{2}} 0^{\frac{n}{2}} | n = N_{m-1}\} \quad (13)$$

$$F_m^{\text{odd}} = \{(01)^{\frac{n}{2}} | n = N_{m-1}\} \quad (14)$$

$$F_m^{\text{even}} = \{(10)^{\frac{n}{2}} | n = N_{m-1}\} \quad (15)$$

$$F_m^{\text{inside}} = \begin{cases} \{0^{\frac{n}{4}} 1^{\frac{n}{2}} 0^{\frac{n}{4}} | n = N_{m-1}\} & \text{if } N_{m-1} > 2 \\ \{01\} & \text{if } N_{m-1} = 2 \end{cases} \quad (16)$$

$$F_m^{\text{outside}} = \begin{cases} \{1^{\frac{n}{4}} 0^{\frac{n}{2}} 1^{\frac{n}{4}} | n = N_{m-1}\} & \text{if } N_{m-1} > 2 \\ \{10\} & \text{if } N_{m-1} = 2 \end{cases} \quad (17)$$

where the exponent  $a^3 \equiv \{a\} \circ \{a\} \circ \{a\} = aaa$  refers to the regular operation concatenation:  $A \circ B = \{xy | x \in A, y \in B\}$ . The pooling filter  $F_{\text{inside}}$  yields 0110, visually this pattern pools qubits from the inside (the middle of the circuit), see Figure 5 (c). Figure 5 (a) shows the repeated usage of  $F^{\text{right}}$  for pooling. This particular pattern is useful for data preprocessing techniques such as principal component analysis (PCA) since PCA introduces an order of importance to the features used in the model. Typically, the first principal component (which explains the most variance) is encoded on the first qubit, the second principal component on the second qubit and so on. Therefore, it makes sense to pool the last qubits and leave the first qubits in the model for as long as possible. If  $N = 8$ ,  $s_c = 1$ ,  $s_p = 0$  and  $F^* = F^{\text{right}}$  then Algorithm 1 generates the circuit in Figure 1 (d), Figure 2, Figure 3 (f) and Figure 5 (a). Specifically Figure 5 show how different values for  $s_c, s_p$  and  $F^*$  generates different instances of the family using Algorithm 1. The possible combinations of  $N, s_c, s_p, F^*$  represent the size of the search space / family. Since  $F^*$  reduces system size in half, it's required that the number of available

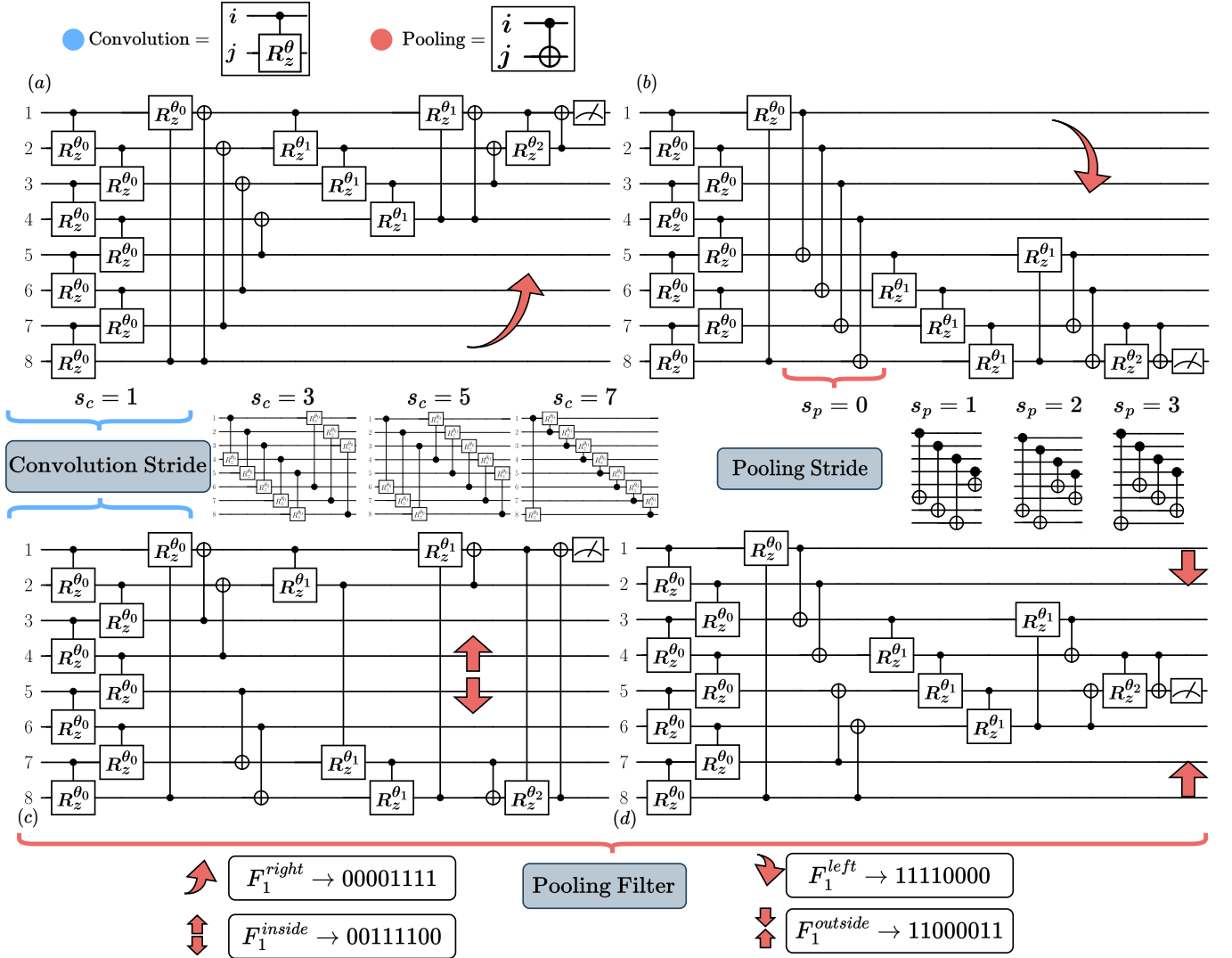


FIG. 5: An example of how the hyperparameters of the primitives effect the circuit architecture of the family generated by Algorithm 1. Three are shown, the convolution stride  $s_c$ , pooling stride  $s_p$  and pooling filter  $F^*$ . These are specified in Section III. Controlled- $R_z^θ$  gates are used for convolutions and CNOTs for pooling as an example. The convolution stride  $s_c$  determine how convolution unitaries are distributed across the circuit. Each convolution primitive typically consist of multiple unitaries and the QCNN requires them to be identical for weight sharing. The pooling stride  $s_p$  determine how pooling unitaries are distributed, for a given pooling primitive, a portion of available qubits gets pooled via controlled unitary operations and  $s_p$  dictates which controls match to which targets. The pooling filter  $F^*$  dictates which qubits to pool according to some recursive pattern/mask. For example, circuit d) always pools the outside qubits during pooling primitives, resulting in the middle qubit making it to the end of the circuit.

qubits  $N$  be a power of two. Using integer strides cause the  $|E_m^c| = |Q_m^c|$  constraint (see section III controlling primitives) which enable translational invariance. The complexity of the model (in terms of number of unitaries used) then scale linearly with the number of qubits  $N$  available. Specifically,  $N$  qubits result in  $3N - 2$  number of unitaries [58].

#### IV. EXPERIMENTAL SETUP

Figure 1 gives a broad view of the machine learning pipeline we implement for the benchmarks. There are various factors influencing model performance during such a pipeline. Each step from raw audio signal to classified musical genre contains a wide range of possible configurations, the influence of which propagates throughout the pipeline. For this reason, it is difficult to isolate any one configuration and evaluate its effect on the model. With our goal being to analyse QCNN

architectures (Figure 1 d) on the audio data, we perform random search in the family created by algorithm 1 with different choices of circuit ansatz and quantum data encoding. These are evaluated on two different datasets: Mel spectrogram data (Figure 1 b) and 2D statistical data (Figure 1 c) both being derived from the same audio signal (Figure 1 a). We preprocess the data based on requirements imposed by the model implementation before encoding it into a quantum state. These configurations are expanded on below:

## Data

For the data component, we aimed to use a practical and widely applicable dataset, and chose the well known [59] music genre dataset, GTZAN. It consists of 1000 audio tracks, each being a 30-second recording of some song. These recordings were obtained from radio, compact disks and compressed MP3 audio files [60]. Each is given a label of one of the following ten musical genres: (**blues, classical, country, disco, hip-hop, jazz, metal, pop, reggae, rock**). Binary classification is used for the analysis of model performance across different architectures. Meaning, there are  $\binom{10}{2} = 45$  possible genre pairs to build models from. Each pair being equally balanced since there are 100 songs for each genre. The dataset therefore enables the comparison of 45 models per configuration within the audio domain.

## Model Implementation

For all experiments, we evaluate instances of Algorithm 1 with  $N = 8$  qubits, resulting in  $3(8) - 2 = 22$  two qubit unitaries. We test each model based on different combinations of model architecture, two qubit unitary ansatz and quantum data encoding. The specific unitaries for  $U_m$  are chosen from a set of eight ansatzes that were used by [28]. They are based on previous studies that explore the expressibility and entangling capability of parameterized circuits [61], hierarchical quantum classifiers [26] and extensions to the VQE [62]. These are shown figure A.1, the ansatz for pooling also comes from [28] and is shown in figure 6. For quantum data encoding, we compare qubit encoding [48] with IQP encoding [63] on the tabular dataset. Amplitude encoding [64] is used for the image data.

Each model configuration considers all 45 genre pairs for classification, for example, rock vs reggae. Cross entropy is used as the cost function  $C(y, \hat{y})$  during training, for rock vs reggae this would be:

$$C(y, \hat{y}) = -(y \log(\hat{y}) + (1 - y) \log(1 - \hat{y})) \quad (18)$$

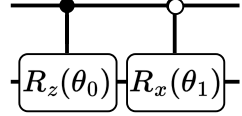


FIG. 6: Pooling ansatz from the experiments of [28]. A rotation is applied on the second qubit based on whether the control is one (filled circle) or zero (open circle).

where

$$y_i = \begin{cases} 1 & \text{if song } i \text{ is labelled rock,} \\ 0 & \text{if song } i \text{ labelled reggae} \end{cases} \quad (19)$$

$\hat{y}_i$  is obtained from equation 4,  $i$  represents one observation and both  $y, \hat{y}$  are all the observations in vector form.

## Data Creation

We benchmark the model against two different forms of data, namely tabular and image. To construct the dataset in tabular form, specific features are extracted from each audio signal using librosa [65] as shown in Figure 1 (b). Each row represents a single audio track with its features as columns. The specific features extracted are those typically used by music information retrieval systems, namely: *chroma frequencies, harmonic and percussive elements, Mel-frequency cepstral coefficients, root-mean-square, spectral bandwidth, spectral centroid, spectral rolloff, tempo and the zero crossing rate*. See Appendix B for a short description these features.

To construct the data set in image form, we extract a mel frequency spectrogram (Figure 1 c) from each audio signal. The mel scale is a non-linear transformation based on how humans perceive sound, and is frequently used in speech recognition applications [66]. The size of the spectrogram we use depends on the number of qubits available for the QCNN. With amplitude encoding, we can encode  $2^N$  values into a quantum state, where  $N$  is the number of available qubits. Using  $N = 8$  qubits, we scale the image down to  $8 \times 32 = 256 = 2^8$  pixels, normalizing each pixel between 0 and 1. The down scaling is done by binning the mel frequencies into eight groups and taking the first three seconds of each audio signal.

## Data Preprocessing

Two main forms of preprocessing are applied to the data before it is sent to the model, namely feature scaling and feature selection. The features are scaled using min-max scaling, where the range is based on the type of quantum data encoding used. With amplitude encoding, the data is scaled to the range  $[0, 1]$ , qubit encoding to  $[0, \pi/2]$  and IQP encoding to  $[0, \pi]$ . Feature selection is only applied to the tabular data. Using qubit encoding

with  $N = 8$  qubits result in selecting eight features. Principal Component Analysis (PCA) and decision trees are used to perform the selection. The tree based selection is used to compare against the PCA, to verify whether the results of the model is not heavily biased by PCA.

### Model Evaluation

The model is trained with 70% of the data while 30% is held out as a test set to evaluate performance. During training five-fold cross validation is used on each model. The average classification accuracy and standard deviation of 30 separate trained instances are calculated on the test set as performance metrics.

## V. RESULTS

To illustrate the impact of architecture on model performance, we compare the fixed architecture from the experiments of Hur et al. [28] to related architectures in the same family, while keeping all other components the same. Meaning the only difference in each comparison is architecture (how the unitaries are spread across the circuit). Within our framework, the architecture in [28] is represented as:  $(s_c, F^*, s_p) = (1, \text{even}, 0) \mapsto \text{Qfree}(8) + (\text{Qconv}(1) + \text{Qpool}(0, F^{\text{even}})) \times 3$ , see algorithm 1. The comparison is performed on the country vs rock genre pair, since it proved to be one of the most difficult classification tasks from the 45 possibilities. We compare eight unitary ansatzes with different levels of complexity, shown in figure A.1.

Architecture vs Ansatz				
Ansatz, # Params	Architecture		Alteration	
	Reference	New alteration	$\Delta$	$(s_c, F^*, s_p)$
A.1a, 6	$65.37 \pm 2.8$	<b><math>75.14 \pm 1.7</math></b>	+9.77	(6, left, 2)
A.1b, 6	$56.34 \pm 3.2$	<b><math>70.46 \pm 1.0</math></b>	+14.12	(1, odd, 3)
A.1c, 12	$52.69 \pm 3.8$	<b><math>70.74 \pm 1.3</math></b>	+18.05	(1, odd, 0)
A.1d, 18	$67.13 \pm 1.5$	<b><math>77.87 \pm 2.4</math></b>	+9.87	(1, outside, 2)
A.1e, 18	$67.87 \pm 2.5$	<b><math>73.61 \pm 1.8</math></b>	+5.74	(6, left, 0)
A.1f, 18	$69.21 \pm 2.6$	<b><math>74.80 \pm 2.8</math></b>	+5.59	(1, left, 3)
A.1g, 30	$73.24 \pm 2.9$	<b><math>79.47 \pm 2.2</math></b>	+6.23	(2, left, 1)
A.1h, 30	$69.35 \pm 4.1$	<b><math>71.71 \pm 3.7</math></b>	+2.36	(2, left, 1)

TABLE I: Country vs Rock average accuracy and standard deviation on a held out test set after 30 separate trained instances. All architectures come from the family of reverse binary trees, algorithm 1. The reference is the architecture used in the experiments of [28] and the alteration was found through random search of the same family. The ansatzes also come from [28] which is based off previous studies benchmarking PQCs [26, 61, 62].

Table I show the result of the comparisons, the reference architecture is as described above and the discovered alteration found via random search. Each value

represents average model accuracy  $\pm$  its standard deviation from 30 separate trained instances on the the same held out test set. Ansatz refers to the unitary used for the convolution operations of a model, for example the model in figure 1 (d) combined with ansatz A.1a means it's used as  $U_1, U_2$  and  $U_3$ . Each model is built with  $N = 8$  qubits and have the same number of unitaries  $3N - 2 \rightarrow 3(8) - 2 = 22$ , 13 of which come from convolutions. Each convolution share weights between its unitary ansatz and there are 3 convolutions for each model. Meaning the number of parameters to optimize is mostly determined by the unitary ansatz for convolutions, for instance, ansatz A.1a has 2 parameters which cause the model to have  $2 \times 3 = 6$  parameters. This illustrates the first important result, which is that model performance can be improved without increasing its complexity. For instance, the best performing model for the reference architecture is with ansatz A.1g obtaining an average accuracy of 73.24%, this ansatz cause the model to have  $10 \times 3 = 30$  parameters. In contrast, by alternating architecture with the simplest ansatz A.1a, it was able to outperform the best reference model with an average accuracy of 75.14%, where it causes the model to only have  $3 \times 2 = 6$  parameters. Another interesting result is for ansatz A.1c, the reference architecture could only obtain an average accuracy of 52.69% indicating its inability to find any kind of local minimum during training, leading one to think it might be a barren plateau. But, the altered architecture was able to find a local minima and improve the average accuracy by 18.05%.

Table II show the performance across the family of reverse binary trees (algorithm 1) for the A.1a ansatz. As mentioned in section III search space design, it's easy to increase and decrease the size of this space. Each value represents the average accuracy of five trained instances on the country vs rock genre pair. The overall accuracy of the whole space is 63.11% indicating that the reference architecture from table I was close to the mean performance. The alteration is part of the best performing architectures  $(s_c, F^*, s_p) = (6, \text{left}, 2)$  with an average accuracy of 75.93. It seems that the combination of  $F^{\text{left}}$  and  $s_c = 6$  perform particularly well for this task, with an average accuracy of 72.52%. In general it seems that the convolution stride  $s_c$  and pooling filter  $F^*$  effect performance the most. It's also worth noting that convolution strides of  $s_c = 3, 4, 5$  performed badly compared to the others. The range of performance goes from a minimum of 43.75% to a maximum of 75.93%, showing the potential impact of the architectural choice.

Finally, we compared the performance of two different architectures on the image data across all genres. This time using ansatz Figure A.1g to compare the  $F_m^{\text{right}}$  and  $F_m^{\text{even}}$  pooling filters, shown in Figures 7 and 8. As mentioned in Section IV, the image data is a low-resolution ( $8 \times 32 = 256 = 2^8$  pixels) spectrogram of the audio signal. We therefore did not expect high accuracy, but were interested in the variation of performance for different architectures. Figures 7 and 8 indicate the

Performance across architecture search space								
	Convolution stride, $s_c$							
$F^*, s_p$	1	2	3	4	5	6	7	Avg
<b>even</b>	<b>67.01</b>	63.63	60.76	64.93	59.98	63.1	59.49	62.81
0	65.97	58.68	56.25	66.67	62.85	59.72	63.43	61.88
1	66.32	66.32	63.54	60.07	61.46	71.88	54.17	63.73
2	66.67	60.76	60.07	68.06	54.17	58.8	63.89	61.81
3	69.1	68.75	63.19	64.93	61.46	60.19	56.48	63.84
<b>inside</b>	66.41	<b>71.96</b>	58.25	54.25	69.27	68.15	60.53	64.18
0	65.28	72.22	60.07	49.65	70.49	68.4	60.65	63.94
1	67.01	71.18	58.68	55.9	66.32	68.4	60.19	64.09
2	68.4	71.53	58.33	51.74	71.88	68.98	58.8	64.26
3	64.93	72.92	55.9	59.72	68.4	66.67	62.5	64.42
<b>left</b>	62.85	61.63	59.38	59.03	51.56	<b>72.52</b>	72.45	62.22
0	66.67	67.01	56.94	61.46	52.08	71.18	73.61	63.79
1	59.03	62.15	52.78	57.99	52.08	71.18	73.61	60.8
2	63.19	63.19	63.19	60.76	51.74	<b>75.93</b>	71.76	63.51
3	62.5	54.17	64.58	55.9	50.35	72.69	70.83	60.79
<b>odd</b>	61.11	<b>68.75</b>	63.37	62.76	64.67	60.52	57.99	62.96
0	60.76	71.88	63.19	58.33	63.54	59.38	57.87	62.29
1	63.54	67.36	64.58	63.54	64.24	62.5	59.26	63.73
2	60.42	70.14	64.58	65.97	69.1	58.8	56.94	64.16
3	59.72	65.62	61.11	63.19	61.81	61.11	57.87	61.65
<b>outside</b>	60.68	65.8	65.54	57.12	62.15	59.83	<b>67.13</b>	62.51
0	67.36	59.72	71.88	54.17	67.01	60.07	70.37	64.15
1	53.47	69.79	62.15	56.25	61.11	58.33	70.83	61.49
2	57.99	70.83	60.07	61.11	59.03	59.26	66.67	62.07
3	63.89	62.85	68.06	56.94	61.46	61.57	60.65	62.29
<b>right</b>	<b>70.05</b>	65.63	64.41	53.65	68.66	63.69	60.65	63.94
0	70.14	63.54	64.58	50	68.4	61.11	62.96	62.96
1	69.79	67.71	64.58	69.1	68.06	67.01	57.87	66.62
2	70.14	62.15	63.89	43.75	68.75	62.04	61.57	61.75
3	70.14	69.1	64.58	51.74	69.44	64.35	60.19	64.37
<b>Avg</b>	64.68	66.23	61.95	58.62	62.72	64.69	63.04	63.11

TABLE II: Country vs Rock average accuracy within the reverse binary tree search space, all with A.1a as ansatz. The convolution stride  $s_c$  is shown on the horizontal axis and the combinations of pooling filter  $F^*$  and stride  $s_p$  on the vertical. The best pooling filter and convolution stride combinations are presented in bold along with the overall best architecture  $(s_c, F^*, s_p) = (6, \text{left}, 2)$ .

difficulty some genre pairs. Interestingly, the  $F_m^{right}$  pooling filter outperformed the  $F_m^{even}$  filter on almost all genres. If we focus on the genre pairs that the models were able to classify, we see that  $F_m^{right}$  had 14 models that achieved an accuracy above 75% compared to the 5 of  $F_m^{even}$ . We also note that the image data had no PCA or tree based feature selection applied on it, and the  $F_m^{right}$  filter was still favoured. A similar result was obtained with the ansatz A.1a.

## VI. OUTLOOK

The main contribution of this paper is a framework enabling the dynamic generation of QCNNs and the creation of QCNN search spaces. It's provided theoretically

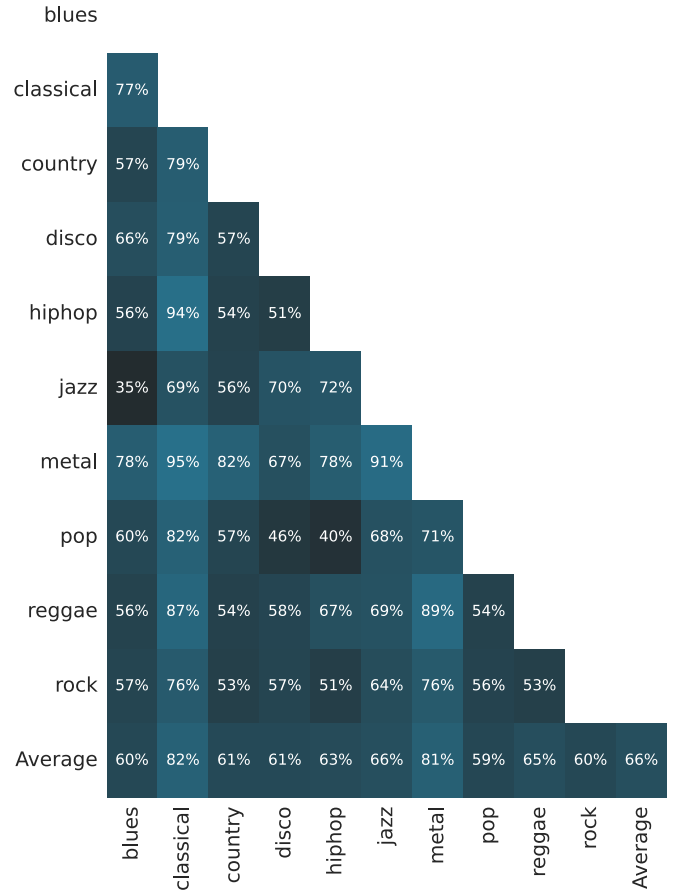


FIG. 7: QCNN with the  $F_m^{right}$  pooling filter using low resolution image data. The accuracies for all genre pairs are provided

in this paper and practically as a python package ready for use. Our experimental results justify the importance of alternating architecture for PQCs, illustrating a means to increase model performance without increasing its complexity. Our next step is to explore search strategies using this architectural representation to automatically find good performing QCNNs for different classification tasks. The method of representation is particularly useful for evolutionary algorithms as shown by [25]. Reinforcement learning and random search algorithms are also applicable. Another interesting consideration is theoretical analysis of QCNN architectures generalizing well across multiple data sets. The framework also allow for different qubit orderings that can correspond to physical hardware setups, therefore benchmarking the effect of noise of different architectures on NISQ devices would be a useful exploration.

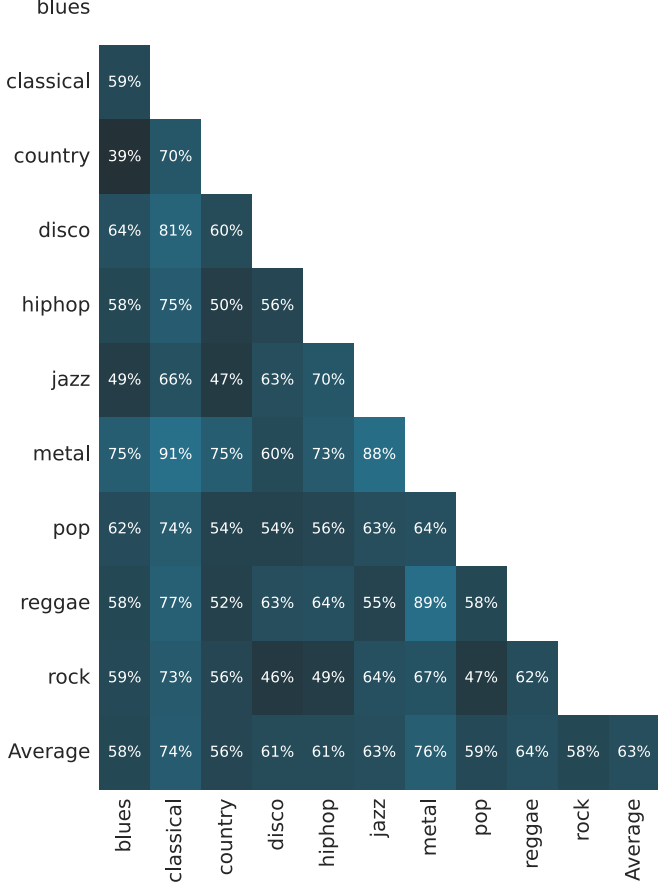


FIG. 8: QCNN with the  $F_m^{even}$  pooling filter using low resolution image data. The accuracies for all genre pairs are provided

## DATA AVAILABILITY

The dataset analysed during the current study is available on TensorFlow Datasets, <https://www.tensorflow.org/datasets/catalog/gtzan>. The source code used to generate QCNNs is available on github as a package, <https://github.com/mattlourens/dynamic-qcnn>.

## ACKNOWLEDGMENT

The development of the python package was funded by Unitary Fund (<https://unitary.fund/>). This research was supported by the Yonsei University Research Fund of 2022 (2022-22-0124), by the National Research Foundation of Korea (Grant Nos. 2019M3E4A1079666 and 2022M3E4A1074591), and by the KIST Institutional Program (2E31531-22-076).

## Appendix A: Circuit ansatz

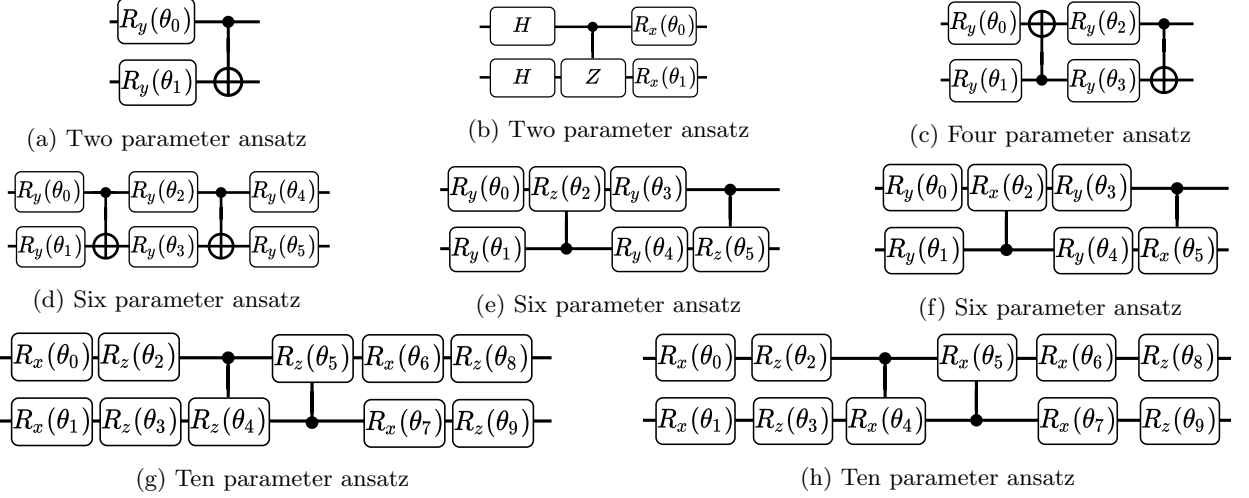


FIG. A.1: The different unitary ansatzes used for the convolution operation  $U_m$  across all experiments. The same ansatzes were used in the benchmarks of [28]. They are based on previous studies that explore the expressibility and entangling capability of parameterized circuits [61], hierarchical quantum classifiers [26] and extensions to the VQE [62].

## Appendix B: Feature Summary

Chroma frequencies	Bins the different pitches of a song into the equal tempered 12-tone scale commonly used in western music.
Harmonic and percussive elements	The harmonic and percussive components present in the signal separated via median filtering.
Mel-frequency cepstral coefficients	Coefficients that make up the mel frequency cepstrum, where mel frequency is the transformation of a signal to the mel scale which characterizes human audio perception. It's commonly used for speech recognition, mobile phone identification and genre classification.
Root-mean-square	The square root of the average of the square of the signal, $\sqrt{\frac{1}{T_2-T_1} \int_{T_1}^{T_2} x(t)^2 dt}$ where $x(t)$ is the amplitude of the signal at time $t$ .
Spectral centroid	The expected value of the frequency spectrum in a time interval. A type of centre of mass which can be used as an indication of tone brightness.
Spectral bandwidth	The standard deviation of the frequency spectrum around its centroid in a time interval.
Spectral rolloff	The frequency bin where the cumulative spectral energy is a specified percentage.
Tempo	The speed of the music, estimated in beats per minute.
Zero crossing rate	The rate at which the amplitude of the signal crosses zero or changes sign.

TABLE III: The information gathered from audio signals to produce the tabular form data set for genre classification benchmarks.

---

[1] Marcello Benedetti, Erika Lloyd, Stefan Sack, and Mattia Fiorentini. Parameterized quantum circuits as machine learning models. *Quantum Science and Technology*, 4(4):043001, nov 2019.

[2] M. Cerezo, Andrew Arrasmith, Ryan Babbush, Simon C. Benjamin, Suguru Endo, Keisuke Fujii, Jarrod R. McClean, Kosuke Mitarai, Xiao Yuan, Lukasz Cincio, and Patrick J. Coles. Variational quantum algorithms. *Nature Reviews Physics*, 3(9):625–644, 2021.

[3] S. Mangini, F. Tacchino, D. Gerace, D. Bajoni, and C. Macchiavello. Quantum computing models for artificial neural networks. *EPL (Europhysics Letters)*, 134(1):10002, April 2021.

[4] Kishor Bharti, Alba Cervera-Lierta, Thi Ha Kyaw, Tobias Haug, Sumner Alperin-Lea, Abhinav Anand, Matthias Degroote, Hermanni Heimonen, Jakob S. Kottmann, Tim Menke, Wai-Keong Mok, Sukin Sim, Leong-Chuan Kwek, and Alán Aspuru-Guzik. Noisy intermediate-scale quantum algorithms. *Rev. Mod. Phys.*, 94:015004, Feb 2022.

[5] Iris Cong, Soonwon Choi, and Mikhail D. Lukin. Quantum convolutional neural networks. *Nature Physics*, 15(12):1273–1278, December 2019.

[6] Arthur Pesah, M. Cerezo, Samson Wang, Tyler Volkoff, Andrew T. Sornborger, and Patrick J. Coles. Absence of barren plateaus in quantum convolutional neural networks. *Phys. Rev. X*, 11:041011, Oct 2021.

[7] Leonardo Banchi, Jason Pereira, and Stefano Pirandola. Generalization in quantum machine learning: A quantum information standpoint. *PRX Quantum*, 2:040321, Nov 2021.

[8] Giuseppe Carleo and Matthias Troyer. Solving the quantum many-body problem with artificial neural networks. *Science*, 355(6325):602–606, 2017. Publisher: American Association for the Advancement of Science.

[9] Juan Carrasquilla and Roger G. Melko. Machine learning phases of matter. *Nature Physics*, 13(5):431–434, 2017.

[10] Evert P. L. van Nieuwenburg, Ye-Hua Liu, and Sebastian D. Huber. Learning phase transitions by confusion. *Nature Physics*, 13(5):435–439, 2017.

[11] Dong-Ling Deng, Xiaopeng Li, and S. Das Sarma. Machine Learning Topological States. *Physical Review B*, 96(19):195145, 2017.

[12] Yoav Levine, Or Sharir, Nadav Cohen, and Amnon Shashua. Quantum Entanglement in Deep Learning Architectures. *Physical Review Letters*, 122(6):065301.

[13] Edwin Stoudenmire and David J Schwab. Supervised Learning with Tensor Networks. In *Advances in Neural Information Processing Systems*, volume 29. Curran Associates, Inc.

[14] Dong-Ling Deng, Xiaopeng Li, and S. Das Sarma. Quantum Entanglement in Neural Network States. *Physical Review X*, 7(2):021021.

[15] Henry W. Lin, Max Tegmark, and David Rolnick. Why does deep and cheap learning work so well? *Journal of Statistical Physics*, 168(6):1223–1247.

[16] Pankaj Mehta and David J. Schwab. An exact mapping between the Variational Renormalization Group and Deep Learning. *arXiv:1410.3831[cond-mat]*.

[17] Yoav Levine, David Yakira, Nadav Cohen, and Amnon Shashua. Deep Learning and Quantum Entanglement: Fundamental Connections with Implications to Network Design. In *International Conference on Learning Representations*.

[18] Yann LeCun, Yoshua Bengio, and Geoffrey Hinton. Deep learning. *Nature*, 521(7553):436–444, May 2015.

[19] Alex Krizhevsky, Ilya Sutskever, and Geoffrey E Hinton. ImageNet Classification with Deep Convolutional Neural Networks. In *Advances in Neural Information Processing Systems*, volume 25. Curran Associates, Inc.

[20] Barret Zoph and Quoc V. Le. Neural Architecture Search with Reinforcement Learning. In *International Conference on Learning Representations*, 2017.

[21] Thomas Elsken, Jan Hendrik Metzen, and Frank Hutter. Neural architecture search: A survey. *The Journal of Machine Learning Research*, 20(1):1997–2017, January 2019.

[22] Esteban Real, Alok Aggarwal, Yanping Huang, and Quoc V. Le. Regularized Evolution for Image Classifier Architecture Search. *Proceedings of the AAAI Conference on Artificial Intelligence*, 33(01):4780–4789.

[23] Barret Zoph, Vijay Vasudevan, Jonathon Shlens, and Quoc V. Le. Learning Transferable Architectures for Scalable Image Recognition. In *Proceedings of the IEEE Conference on Computer Vision and Pattern Recognition*, pages 8697–8710, 2018.

[24] Liang-Chieh Chen, Maxwell Collins, Yukun Zhu, George Papandreou, Barret Zoph, Florian Schroff, Hartwig Adam, and Jon Shlens. Searching for Efficient Multi-Scale Architectures for Dense Image Prediction. In *Advances in Neural Information Processing Systems*, volume 31. Curran Associates, Inc.

[25] Hanxiao Liu, Karen Simonyan, Oriol Vinyals, Chrisantha Fernando, and Koray Kavukcuoglu. Hierarchical Representations for Efficient Architecture Search. In *International Conference on Learning Representations*.

[26] Edward Grant, Marcello Benedetti, Shuxiang Cao, Andrew Hallam, Joshua Lockhart, Vid Stojovic, Andrew G. Green, and Simone Severini. Hierarchical quantum classifiers. *npj Quantum Information*, 4(1):65, December 2018.

[27] Tobias Haug, Kishor Bharti, and M.S. Kim. Capacity and quantum geometry of parametrized quantum circuits. *PRX Quantum*, 2(4):040309. Publisher: American Physical Society.

[28] Tak Hur, Leeseok Kim, and Daniel K. Park. Quantum convolutional neural network for classical data classification. *Quantum Machine Intelligence*, 4(1):3.

[29] Seunghyeok Oh, Jaeho Choi, and Joongheon Kim. A Tutorial on Quantum Convolutional Neural Networks (QCNN). In *2020 International Conference on Information and Communication Technology Convergence (ICTC)*, pages 236–239.

[30] Lukas Franken and Bogdan Georgiev. Explorations in quantum neural networks with intermediate measurements. In *ESANN*, pages 297–302, 2020.

[31] Jarrod R. McClean, Sergio Boixo, Vadim N. Smelyanskiy, Ryan Babbush, and Hartmut Neven. Barren plateaus in quantum neural network training landscapes. *Nature Communications*, 9(1):4812.

[32] Zoë Holmes, Kunal Sharma, M. Cerezo, and Patrick J. Coles. Connecting Ansatz Expressibility to Gradient Magnitudes and Barren Plateaus. *PRX Quantum*,

3(1):010313.

[33] Maria Schuld, Ryan Sweke, and Johannes Jakob Meyer. Effect of data encoding on the expressive power of variational quantum-machine-learning models. *Physical Review A*, 103(3):032430.

[34] Amira Abbas, David Sutter, Christa Zoufal, Aurélien Lucchi, Alessio Figalli, and Stefan Woerner. The power of quantum neural networks. *Nature Computational Science*, 1(6):403–409.

[35] Maria Schuld. *Quantum Machine Learning Models Are Kernel Methods*.

[36] Shi-Xin Zhang, Chang-Yu Hsieh, Shengyu Zhang, and Hong Yao. Differentiable quantum architecture search. *Quantum Science and Technology*, 7(4):045023, aug 2022.

[37] Shi-Xin Zhang, Chang-Yu Hsieh, Shengyu Zhang, and Hong Yao. Neural Predictor based Quantum Architecture Search. *Machine Learning: Science and Technology*, 2(4):045027.

[38] Harper R. Grimsley, Sophia E. Economou, Edwin Barnes, and Nicholas J. Mayhall. An adaptive variational algorithm for exact molecular simulations on a quantum computer. *Nature Communications*, 10(1):3007.

[39] Ho Lun Tang, V.O. Shkolnikov, George S. Barron, Harper R. Grimsley, Nicholas J. Mayhall, Edwin Barnes, and Sophia E. Economou. Qubit-ADAPT-VQE: An Adaptive Algorithm for Constructing Hardware-Efficient Ansatz on a Quantum Processor. *PRX Quantum*, 2(2):020310.

[40] Yordan S. Yordanov, V. Armaos, Crispin H. W. Barnes, and David R. M. Arvidsson-Shukur. Qubit-excitation-based adaptive variational quantum eigensolver. *Communications Physics*, 4(1):228.

[41] Arthur G. Rattew, Shaohan Hu, Marco Pistoia, Richard Chen, and Steve Wood. A Domain-agnostic, Noise-resistant, Hardware-efficient Evolutionary Variational Quantum Eigensolver.

[42] Linghua Zhu, Ho Lun Tang, George S. Barron, F. A. Calderon-Vargas, Nicholas J. Mayhall, Edwin Barnes, and Sophia E. Economou. Adaptive quantum approximate optimization algorithm for solving combinatorial problems on a quantum computer. *Physical Review Research*, 4(3):033029.

[43] Li Li, Minjie Fan, Marc Coram, Patrick Riley, and Stefan Leichenauer. Quantum optimization with a novel Gibbs objective function and ansatz architecture search. *Physical Review Research*, 2(2):023074.

[44] Mateusz Ostaszewski, Edward Grant, and Marcello Benedetti. Structure optimization for parameterized quantum circuits. *Quantum*, 5:391.

[45] Yuxuan Du, Tao Huang, Shan You, Min-Hsue Hsieh, and Dacheng Tao. Quantum circuit architecture search for variational quantum algorithms. *npj Quantum Information*, 8(1):1–8.

[46] John Preskill. Quantum Computing in the NISQ era and beyond. *Quantum*, 2:79, August 2018.

[47] Jarrod R. McClean, Jonathan Romero, Ryan Babbush, and Alán Aspuru-Guzik. The theory of variational hybrid quantum-classical algorithms. *New Journal of Physics*, 18(2):023023.

[48] Maria Schuld. Supervised quantum machine learning models are kernel methods.

[49] Román Orús. A practical introduction to tensor networks: Matrix product states and projected entangled pair states. *Annals of Physics*, 349:117–158.

[50] William Huggins, Piyush Patel, K. Birgitta Whaley, and E. Miles Stoudenmire. Towards Quantum Machine Learning with Tensor Networks. *Quantum Science and Technology*, 4(2):024001.

[51] Ian Goodfellow, Yoshua Bengio, and Aaron Courville. *Deep Learning*. MIT Press, 2016. <http://www.deeplearningbook.org>.

[52] Iordanis Kerenidis, Jonas Landman, and Anupam Prakash. Quantum algorithms for deep convolutional neural networks. *arXiv:1911.01117[quant-ph]*, 2019.

[53] YaoChong Li, Ri-Gui Zhou, RuQing Xu, Jia Luo, and WenWen Hu. A quantum deep convolutional neural network for image recognition. *Quantum Science and Technology*, 5(4):044003, July 2020.

[54] Maxwell Henderson, Samriddhi Shakya, Shashindra Pradhan, and Tristan Cook. Quanvolutional neural networks: powering image recognition with quantum circuits. *Quantum Machine Intelligence*, 2(1):2, June 2020.

[55] ShiJie Wei, YanHu Chen, ZengRong Zhou, and GuiLu Long. A Quantum Convolutional Neural Network on NISQ Devices. *arXiv:2104.06918 [quant-ph]*, April 2021. arXiv: 2104.06918.

[56] Michael A. Nielsen and Isaac L. Chuang. *Quantum Computation and Quantum Information: 10th Anniversary Edition*. Cambridge University Press, New York, NY, USA, 10th edition, 2011.

[57] These are 0011,1100,1010,0101,0110,1001, equal in the sense that they have the same number of 1s and 0s.

[58] This is because of the geometric series:  $N(\frac{1}{2^0} + \frac{1}{2^1} + \cdots + \frac{1}{2^{\log_2 N-1}}) + N(\frac{1}{2^1} + \frac{1}{2^2} + \cdots + \frac{1}{2^{\log_2 N-1}})$ . Where the first sum is for convolution unitaries and the second for pooling.

[59] Bob L. Sturm. A Survey of Evaluation in Music Genre Recognition. In Andreas Nürnberg, Sebastian Stober, Birger Larsen, and Marcin Detyniecki, editors, *Adaptive Multimedia Retrieval: Semantics, Context, and Adaptation*, volume 8382 of *Lecture Notes in Computer Science*, pages 29–66. Springer International Publishing.

[60] Tzanetakis George, Essl Georg, and Cook Perry. Automatic musical genre classification of audio signals. In *Proceedings of the 2nd international symposium on music information retrieval, Indiana*, volume 144, 2001.

[61] Sukin Sim, Peter D. Johnson, and Alán Aspuru-Guzik. Expressibility and entangling capability of parameterized quantum circuits for hybrid quantum-classical algorithms. *Advanced Quantum Technologies*, 2(12):1900070, 2019.

[62] Robert M. Parrish, Edward G. Hohenstein, Peter L. McMahon, and Todd J. Martínez. Quantum computation of electronic transitions using a variational quantum eigensolver. *Phys. Rev. Lett.*, 122:230401, Jun 2019.

[63] Vojtech Havlíček, Antonio D. Córcoles, Kristan Temme, Aram W. Harrow, Abhinav Kandala, Jerry M. Chow, and Jay M. Gambetta. Supervised learning with quantum-enhanced feature spaces. *Nature*, 567(7747):209–212, 2019.

[64] Maria Schuld and Francesco Petruccione. *Machine Learning with Quantum Computers*. Springer International Publishing, 2021-01-01.

[65] Brian McFee, Alexandros Metsai, Matt McVicar, Stefan Balke, Carl Thomé, Colin Raffel, Frank Zalkow, Ayoub Malek, Dana, Kyungyun Lee, Oriol Nieto, Dan Ellis, Jack Mason, Eric Battenberg, Scott Seyfarth, Ryuichi Yama

mamoto, viktorandreevichmorozov, Keunwoo Choi, Josh Moore, Rachel Bittner, Shunsuke Hidaka, Ziyao Wei, nullmightybofo, Darío Hereñú, Fabian-Robert Stöter, Pius Friesch, Adam Weiss, Matt Vollrath, Taewoon Kim, and Thassilo. librosa/librosa: 0.8.1rc2, May 2021.

[66] S. Davis and P. Mermelstein. Comparison of parametric representations for monosyllabic word recognition in continuously spoken sentences. *IEEE Transactions on Acoustics, Speech, and Signal Processing*, 28(4):357–366.